Journal of Scientific Research
Banaras Hindu University, Varanasi

Vol. 63, 2019 : 249-264
ISSN : 0447-9483

CHARGE MEASUREMENT / ESTIMATION TECHNIQUES IN NUCLEAR EMULSION DETECTOR

M. K. Singh[1#], V. Singh[1*], K. Saraswat[1,3], D. Grover[1], Manoj Kumar Singh[1,2], A. Kumar[1], N. Marimuthu[1], A. Pandey[1], P. Kumar[1], R. Prajapati[1,4], D. Singh[1]

1. Department of Physics, Institute of Science, Banaras Hindu University, Varanasi - 221 005, India
2. Institute of Physics, Academia Sinica, Taipei – 111529, Taiwan
3. Physics Department, Kumaun University, Nainital – 263001, India
4. T. D. P. G. College Jaunpur 222002, India

Present Address: Department of Physics, Institute of Applied Sciences & Humanities, G. L. A. University, Mathura - 281406, India

*E-mail address: venkaz@yahoo.com, venktesh@bhu.ac.in

Abstract:

This manuscript provides detailed description related to the measurement techniques frequently used in the nuclear emulsion detector to extract the valuable information related to the nuclear events. With the help of obtained information, charge, momentum and identification of the particle produced or fragments of the projectile and target will be derived. This article also sheds some light on the advanced techniques developed recently for the improvement and better use of the nuclear emulsion detector in the era of modern science.

Keywords: Nuclear Emulsion Detector (NED), Multiplicity measurement and distribution, Charge estimation, Angular measurement, Automatic scanning system.

1. Introduction

Radioactivity discovered in the year 1896 by its effect on photographic film and nuclear emulsions, later played pivotal role in cosmic-ray research such as, in the discovery of pion in 1947. Emulsions continue to be useful in the study of production and decay of short-lived particles produced in high-energy particle physics experiments. Before the operation of high-energy accelerators at CERN, Chicago, Dubna and heavy-ion accelerator at Berkeley in California (USA), most of the basic knowledge on fundamentals of particles interaction came from the studies of cosmic-ray physics using Nuclear Emulsion Detector (NED), Bubble Chamber (BC) and Cloud Chamber (CC).

Projectile fragmentation is a well-established technique for the production of rare isotope beams used by many radioactive ion-beam facilities around the world [1-5]. Even though, the pioneering fragmentation experiments were performed more than 70 years ago in Berkeley [3-5], USA, however, the reaction mechanism of projectile fragmentation is not well understood. Some simplified characteristics have been observed at high energy interactions such as in peripheral and quasi-central collisions [6-10]. Fragment emission angle has been recognized to be a common feature of heavy-ion interactions at intermediate and higher energy for many decades [11-13]. Their importance is confirmed by the fact that it continues to be the subject of intense experimental and theoretical studies [14-19].

The NED is in general made up of gelatin as a basic medium in which projectile or particles moves. The basic elements of the NED composition are Hydrogen (^{1}H), Carbon (^{12}C), Nitrogen (^{14}N), Oxygen (^{16}O), Bromine (^{82}Br) and Silver (^{108}Ag). Their percentage slightly varies according to the basic requirements of the experiments and manufacturing companies such as Ilford G5, Ilford C2, and NIKFI BR2 etc. However, the NED used by us was from NIKFI Company and type BR2. Its general compositions in terms of atoms per cubic centimeter (x10^{22}) of the NED are ^{1}H (3.150), ^{12}C (1.410), ^{14}N (0.395), ^{16}O (0.956), ^{80}Br (1.028) and ^{108}Ag (1.028), and small mixture of Iodine and Florien.

The interesting feature of heavy-ion interactions is the variation of reaction properties with the collision geometry. There are three types of collision classified according to the geometry namely, peripheral, quasi - central and central collisions. The impact parameter (b), defined as the transverse distance between the core of projectile and target nucleus, determines the class of reactions. (I) In case of peripheral collisions having impact parameter b = $R_P + R_T$, where R_P and R_T are the radius of projectile and target nucleus, respectively. In this case, only small momentum is transferred between interacting nuclei during the collision. (II) In case of quasi-central collision the impact parameter (b) is defined as ($| R_P + R_T | > b \geq | R_P - R_T |$), and (III) in case of the central collision, where the impact parameter (b) is defined as ($0 \leq b < | R_P - R_T |$). The number of nucleons taking part in the quasi-central and central collisions is large compared to that of peripheral collisions. In central collision a large amount of energy or momentum is transferred from projectile to the target nucleus. A schematic diagram as shown in **Figure 1**, displays these concepts in terms of impact parameter (b) and the right hand side have microscopic images of each type of collisions in the laboratory frame observed for interaction of 1 A GeV $^{84}Kr_{36}$ with the NED nuclei [20].

A simple portrayal of projectile fragmentation process is shown in **Figure 2**, the overlapping region of target and projectile is sheared off, leaving an excited pre-fragment compound nucleus. The pre-fragment compound nucleus then de-excites through further decay or statistical emission and becomes the final observed fragments. Due to the differences in physical nature of two processes, one usually uses separate theoretical models to describe the two individual steps of fragmentation [20].

The NED is important because of its basic property of keeping tracks imprint permanent i.e. track image will not change with time. It also presents visual information about the tracks of the charged particle. Due to these two basic features, the NED is still in use in the modern era of science. Nowadays, scientists are proposing many experiments based on the NED for rare physics events search in which search of dark matter candidates is one of them.

2. Latent Image Formations of Charged Particles

The development of latent image formation in an ordinary photographic film and in the NED is almost same. The basic difference in the latent image formation is the mechanism of ion-pair formation. In case of NED, mechanisum is based on the

electrostatic interactions between the incident charge particles and electrons of the NED's atoms. However, in case of photon senstitive photographic film, the mechanisum is based on the photo electron emission due to the photon interactions with matter through photoelectric emission process [20].

Ionizing charged particles, which happen to pass through such NED leave behind a number of silver bromide crystals that have been so altered that, upon development, they appear as lines of black grains of colloidal silver and identify the trajectories of the particles as shown in **Figure 3a**. Figure 3a, represents a schematic diagram of the emulsion latent image formation as it may actually be, and indicates the path of the charged particle passing through it. Here shaded part indicates the crystal, which is activated when charged particle was passed and **Figure 3b**, shows the same track after development. Each activated crystal has grown to roughly twice the original size and undeveloped other crystals have dissolved in the developer solution [21, 22]. The more strongly ionizing charged particles, the more numerous are these grains and the greater their initial energies, and longer the resulting tracks will be developed according to the Bathe-Bloch formula [23].

The Gurney-Mott theory [24] suggests that the formation of latent image may occur in two steps. First step is characterized by the motion of negatively charged electrons in the silver bromide (Ag Br) crystals and the second step is based on the motion of the ions. Passes of incident charged particle initially raised the energy level of few electrons of bromine ions to the vacant states in the conduction band of each crystal. Raised energy state electrons move freely inside the crystal until they are trapped. The trapping position is often called as sensitive specks. These sensitive specks are localized energy levels below the conduction band. These sensitive specks are actually impure atoms or clumps of silver and are located on the crystal surface. The formation of sensitive specks is due to the slow diffusion of the excess bromine on the crystal surface. The sensitive specks attract interstitial silver-ions due to their negative nature. Now they are free to move inside the crystal lattice and combine with the electrons there and form the silver atoms. Sufficient size silver specks act as development centers, which are formed by the repetition of the process during the exposure [20] as shown in the **Figure 4**.

3. Classifications of Target Fragments

The mean number of fully developed and well separated grains per unit length is called the grain density (g). It is a measure of the rate of energy loss of charged particle. The grain density of a track corresponds to a particular specific ionization but its actual value depends on the degree of development of the emulsion and the type of emulsion used. It is therefore, necessary to introduce another quantity called normalized grain density, which is defined as $g^* = g / g_{min}$. Here g is the observed grain density and g_{min} represents the minimum grain density developed due to singly charged particles.

All charged secondary particles emitted or produced in an interaction are classified in accordance with their ionization in terms of normalized grain density; range and velocity into the following categories as given bellow [20].

3 .1 Shower Particle (N_s)

These are freshly created particles having normalized grain density $g^* \leq 1.4$ and relative velocity $\beta \geq 0.7$. They are mostly fast pions with a small admixture of kaons and released protons from the projectile, which have undergone an interaction. The number of such particles is denoted by N_s. These particles usually come from the participant region of the collision and their larger number is a measure of fireball and its collision geometry [20].

3.2 Grey Particle (N_g)

The particle having normalized grain density (g*) in between 1.4 and 6.8, and range (L) more than 3 mm are defined as grey particles. These particles have relative velocity (β) in between 0.3 and 0.7. Generally, they are knocked out protons from the targets having energy (E_P) in the range of 30 and 400 MeV. The number of such particles in an interaction is denoted by N_g. The larger number of such particles in an interaction represents abrupt destruction of target nucleus.

3.3 Black Particle (N_b)

The particle having normalized grain density (g*) more or equal to 6.8 and range (L) less or equal to 3 mm inside the NED are defined as black particles. These particles have relative velocity (β) always less or equal to 0.3. They are basically low energy (E_P < 30 MeV) protons of the target nucleus. Most of these particles are produced owing to evaporation of residual target nucleus. The numbers of such particles in an interaction is denoted by N_b and represent the momentum transfer to the target nucleus from the projectile.

Because of both type (N_g) and (N_b) of particles are coming out from the target nucleus therefore, their sum is collectively called as heavily ionizing charged particle (N_h), also known as the target fragments. The Heavily ionizing charged particle is $N_h = N_b + N_g$.

4. Classifications of Projectile Fragments (PFs)

These are the spectator parts of the projectile nucleus with charge $Z \geq 1$ and having velocity close to the beam velocity. Due to this reason, the ionization of projectile fragments is nearly constant over a few mm of its range and emitted within a highly collimated narrow forward cone whose solid angle depends upon the available beam energy. The forward angle is the angle whose tangent is the ratio of the average transverse momentum of the projectile fragments ($P_{fT} = P_T$) to the longitudinal momentum P_L of the beam. Taking P_L as the beam momentum itself, i.e.,

$$\theta_F = tan^{-1}\left(\frac{P_T}{P_L}\right). \quad (1)$$

The projectile fragmentation is further classified into three categories as mentioned bellow:

4.1 Singly Charged Projectile Fragments ($N_{Z=1}$)

The projectile fragments, which have velocity nearly equal to the initial beam velocity and their specific ionization i.e. energy loss per unit length may be used directly to estimate their charge. The number of such particles in an interaction is denoted by $N_{Z=1}$.

4.2 Alpha Projectile Fragments (N_α)

The projectile fragments having charge Z = 2 are defined as alpha projectile fragments or helium nucleus and the number of such particles in an interaction is denoted by N_α. They can shed light on various physics phenomenon. Their emission process is still not well understood [20].

4.3 Heavy Projectile Fragments (N_f)

These projectile fragments having charge $Z \geq 3$ and the number of such particles in an interaction are denoted by N_f. Their number and its angular correlation can shed light on the various nuclear and astrophysics problems such as fragmentation, multi-fragmentation, short lived fragments etc.

Multiplicity is defined as the number of particles present or produced in a final state of an event or interaction. Therefore, the total multiplicity of the secondary charged particles (N_{ch}) is taken as the sum of all charged particles projected in an interaction, $N_{ch} = N_s + N_g + N_b + N_f + N_{Z=2} + N_{Z=1.}$

5. Experimental Techniques Used for Charge Estimation

When any charged particle passes through the medium, it transfers partial or total energy to the atoms / molecules of the surrounding medium due to interactions or scattering. If the transferred energy is large enough to make the outer most orbital electron free and it makes the medium ionized. The rate of ionization depends on the square of the charge and inverse of the square of the relative velocity of the ionizing particle. Ionization measurements are a great help in the estimation of the charge of the projectile fragments. When the ionization is low, the error in such estimation may not be large while when the grain density increases, the adjacent grain becomes unresolved even under a high magnification microscope due to which the uncertainty increases in the estimation. In case of higher charged tracks the grains get clogged to each other to form blobs and it is not possible to count the individual grains. Since, one method of charge estimation will not be suitable and valid for the wider range of charge fragments; therefore, different methods for a quantitative measurement of the rate of energy loss have been devised and are described in detail as given below [25];

5.1 Blob Density Method

A blob is defined as a single structure or a set of grains clogging to each other and the gap between two adjacent blobs is called a hole. The number of blobs (holes) per 100 μm is called blob (hole) density and represented by B and H, respectively, in this case. If the ionization is small, the blob density is a good parameter to resolve the charge of the particles track. But in case of particles with heavier charge, the blob density decreases rapidly. The distribution of blob density is shown in **Figure 5**. Figure 5 reveals that first it increases up to charge Z = 2 and then drops as blobs continue to collapse into larger blobs. Thus for very large ionization, blob density method is not sensitive. Hence, it can be applied over only a limited range of ionization. After the measurement of the B and H for the projectile fragments which have charge Z = 1, 2 and 3. The variation of B and H versus of Z^2 are shown in **Figure 5 & 6**, respectively [25]. Therefore, B and H measurements alone can't determine the charge over the entire range of ionization.

5.2 Gap-Length Coefficient Method

Gap-length is defined as the distance between the two successive blobs, which is related to the ionization caused by the charged particle. The ratio of the total number of observable gaps to the number of gaps greater than a certain optimum value or the negative slope, G, of the log of frequency distribution of gap-length is a measure of the grain density and is called the Gap-Length Coefficient (G). The gap-length coefficient (G) of the exponential is nearly proportional to the rate of the energy loss of ionizing particle and is obtained using the Fowler-Perkins [26-28] relation as written in Eq. (2),

$$G = -1/L \ln(B/H). \quad (2)$$

For considerably low ionization, one may also find the Gap-length Coefficient from blob density alone by the following relation as written in Eq. (3),

$$B = G \, exp\,(-\alpha.G). \quad (3)$$

Here α is the mean diameter of a developed grain [29-33]. For projectile fragments whose charge could be estimated with this method with one charge unit confidence is up to Z = 8. The variation of computed G for $^{84}Kr_{36}$ projectile versus Z^2 is shown in **Figure 7** [25].

According to Fowler [34-39], the optimum value of L occurs when GL ~ 2.0 for all values of G. The accuracy does not vary appreciably in the interval 1.5 < GL > 2.5. The statistical error in G can be expressed as written in Eq. (4),

$$\frac{dG}{G} = \frac{1}{\sqrt{\left(N_H \ln\left(\frac{B}{H}\right)\right)}}. \quad (4)$$

Where, N_H is the number of gaps greater than the length L. Minimization in error has been done by setting according to Eq. (5),

$$\frac{d}{dH}\sqrt{Hlog\left(\frac{B}{H}\right)}. \tag{5}$$

Solving the differential equation one finds that, $ln\left(\frac{B}{H}\right)$ = 2.0 or $\left(\frac{B}{H}\right)$ = 7.4. The estimation or error is quite reliable as long as $\left(\frac{B}{H}\right)$ > 4 and $N_B > 4$ (N_H) [25].

The measurement of the gap-length coefficient was reported for the fragments ^{84}Kr projectile for ~500 interactions at 1 A GeV [25]. Consider that all the gaps greater than one division of the microscope scale fitted in the eyepiece is equal to L. The calibrated value of 1 division is equal to 0.98 μm i.e. is the least count of instrument in position measurement. However, there was no significant change observed in the results by varying the value of L, since the measurement for each track is based on the counting of a large number of blobs and gaps and also the selection criteria for the charge measurement is responsible for the different values of B and H.

5.3 Delta-Ray Density Method

In a sensitive nuclear emulsion detector, a particle moving at relativistic velocity shows a narrow, dense central core around the trajectory of the primary particle and a number of delta rays, which become numerous as the value of the charge of a primary particle increases. This method is suitable for particles (fragments) with Z > 10, the tracks of which have virtually no gaps, consistent in measuring the number or track lengths of δ-electrons produced by a charged particle as it ionizes the substance along its track. δ-rays are generally knockout electrons having kinetic energy more than 5 keV. This method is based on the fact that the energy and range distributions of δ - electrons are dependent on charge (Z) of the ionizing particle [25, 40-42] according to Eq. (6),

$$\frac{d^2N}{dT\,dx} = \frac{1}{2}(4\pi N_A r_e^2 m_e c^2 Z^2)\left(\frac{Z}{A}\right)\left(\frac{1}{\beta^2}\right)\left(\frac{F}{T^2}\right). \tag{6}$$

Where, T is the kinetic energy of δ - electrons, x is the thickness of the substance passed by the ionizing particle, A is the atomic weight of atoms in the substance, Z is the charge of atoms in the substances, β = (v/*c*), v is the velocity of the ionizing particle, c is the velocity of light, N_A is the Avogadro's number, F is the parameter dependent on the spin of the ionizing particle at relativistic velocities, it is considered to be constant, m_e is the mass of electron and r_e is the classical radius of electron. The second term of right hand side is equal to 0.3071 MeVcm^2g^{-1} [25].

The number of the electrons having kinetic energy more than 5 keV, which escape from the parent particle may produce recognizable delta shape (δ) tracks with three or more than three grains inclined against the direction of the parent particle track. The delta-rays having above criteria will contribute to the value of the delta-ray

density. According to the Demers and Rossi [43, 44], at relativistic velocity, the maximum energy of knockout electrons becomes large compared to any practical minimum delta-ray energy. So the number of delta-rays exceeding a particular minimum energy W_{min} will become N_δ and which is defined as and mentioned in Eq. (7),

$$N_\delta = 2R_0^2 \left(\frac{mc^2}{W_{min}}\right) Z^2. \quad (7)$$

Here m and c is the mass of electron and velocity of light in vacuum, respectively. Generally, we have to choose a fixed value of W_{min} for an experiment. In the above equation, right hand side is constant except Z. Therefore, the delta - ray density ($N_{\delta)}$ is proportional to the square of the particles charge (Z^2). Method developed for determining the particle charge in the detector requires a suitable calibration curve to be plotted based on the measured characteristics of the tracks produced by particles with known charges [25].

If we know the delta-ray density of the known charge particles and that acts as a calibration for the experiment as shown in **Figure 8**. Then, from the Figure 8, the constant for a particular counting convention is determined empirically for the particle of known charges, and the charge of the other relativistic charged particles can be estimated with good accuracy. According to Tidmen et al [45-47], grains configuration to be counted as delta-rays, must attain a minimum displacement of 1.5 micron from the axis of track projected on the plane of the NED. Dependence of delta-ray density on the particle charge is also shown in **Figure 8**. For nuclei having charge Z >19, the number of delta-rays becomes very large and therefore, it is difficult to count their number reliably. Thus, by using this method, we can measure the charge of the projectile fragments in the range 9 < Z < 19. This can vary, depending upon the sensitivity of the NED [25].

5.4 Relative Track-Width

When the ionization caused by projectile fragments is high, most of the information about the charge of the particle can be obtained by measurements of the width of the track formed by the fragment and projectile. The width of the track increases with increase in grain density just in the region where little information remains in the linear track structure. This method is very accurate for the estimation of charge of the heavier fragments (fragments having charge 19 < Z < 30). In this method, we do the measurement of width of the beam and associated fragments at more than four different points just before and after the interaction vertex with the help of the filar micrometer. A filar micrometer is a device generally used to achieve high precision in the measurements. It consists of a micrometer and a reticle that has two fine parallel wires or threads that can be moved by the observer using a screw mechanism. For measuring the width, only the core part of the track has always been chosen to avoid fluctuation in the measurement owing to the delta-rays and the core of the tracks are fixed. The mean width of the fragments to the mean width of the beam

track ratio multiplied by the beam charge gives the accurate estimation of charge of the heavier fragments. The charge of such type of fragments must be duly checked by the charge of the fragments created due to electromagnetic dissociation of the projectile.

5.5 Residual Range Method

The heaviest projectile fragments in some interactions, mostly peripheral collisions, have an appearance almost identical to the beam so far as ionization is concerned. Their charge must thus be only a few units less than the beam charges. Such projectile fragments must be followed from the interaction vertex through the successive pellicles. The residual range method usually adopted for estimating the charge in the range $Z \geq 30$. The residual range in case of the $^{84}Kr_{36}$ - nuclei at the entrance edge is around 7.8 cm [25]. The range of heavy-ion of mass (M) times the proton and charge Z is related to the range of a proton of same velocity by the relation [48-50] as written in Eq. (8),

$$R_z = \left(\frac{M}{Z^2}\right) R_{proton} . \quad (8)$$

Above mentioned method is also applicable for the charge estimation of dissociation type or elastic interactions and found the residual ranges for different charges close to the beam charge. These residual ranges act as reference ranges and with their help approximate assignment of charge to the heaviest projectile fragments in the intervals of $Z \geq 30$ could be done [25].

The average number of projectile fragments measured in the present experiment is tabulated in **Table 1** under three category light, alpha and heavy fragments along with results obtained from other experiments having similar projectile energy. From table 1, one can understand that the projectile fragmentation dependents on the mass number of the projectile except ^{56}Fe projectile.

6. Angular Measurement

In this experiment magnetic field was not used, therefore the particles produced after interaction move in the 4π direction but particle emitted or fragmented from the projectile moves in the forward direction. To know the mechanism of projectile fragmentation and other related nuclear physics we must have to measure the angle of each tracks involved in the interaction. The procedures for angular measurements of the secondary tracks associated with interaction especially projectile fragments are described below [25].

First of all, we have to locate the interaction on the centre of the eyepiece scale i.e. at the cross-wire. After fine focusing the z-axis of microscope, we classify the charge secondary by counting the grain density of each secondary track up to a limited field of view. The angle measurement of projectile fragment should be done in the narrow forward cone of the projectile fragments (PFs). Before starting the angle measurement of PFs, the micrometer scale inside the eyepiece is aligned along the X-

axis of the coordinate. When the micrometer scale becomes aligned with the help of the grains, we align the incident beam tracks along the X-axis of the coordinate by rotating the mechanical stage of the binocular microscope gently. When the beam track as well as micrometer scale become aligned, the interaction vertex is focused at the centre of the field of view of the micrometer scale so that the coordinates of the interaction vertex are recorded as X = 0, Y = 0 and Z = Z_0. Now, we shift the interaction vertex to one end of the scale through a certain known distance as shown in Figure 9, and the two coordinates (X_T and Y_T) of the segment of the PF have been read from the counter display of the digitizing encoder and the third coordinate (Z_T) has been accurately recorded.

The spatial configuration of each event was reconstructed by measuring a set of X, Y and Z coordinates separated by at least 100 μ*m*, along x direction for the incident beam track and of each PF. In other words, coordinate method was used and two point measurement on the beam tracks as well as PFs, by straight line fitting on a particular secondary as well as the beam track should be recorded. We obtain the projected angle of the secondary track (Q_P) in x - y plane (i.e. plane of emulsion) as given in Eq. (9),

$$Q_p = tan^{-1}\left(\frac{y_2-y_1}{x_2-x_1}\right). \quad (9)$$

The dip angle i.e. angle of track in z - y plane or plane perpendicular to the emulsion plane, (Q_d) is given in Eq. (10),

$$Q_d = tan^{-1}\left(\frac{(\Delta Z \times S)}{(\Delta x^2 - \Delta y^2)}\right). \quad (10)$$

Where, ΔZ is the change in Z - axis coordinate in a distance x and y in the (x - y) plane. S is the shrinkage factor. During processing, after exposure of the emulsion, thickness reduced by few factors. So the ratio of thickness of NED before and after the processing is called shrinkage factor (S). Generally the thickness of the NED before processing is around 600 μm but it varies and depends on the type and company of the emulsion film.

The space angle (Q_s) is given in Eq. (11),

$$Q_s = cos^{-1}\left(\frac{cos\theta_p}{\sqrt{1+tan^2\theta_d}}\right). \quad (11)$$

The angle of other type of secondary particle tracks can be measured by the Goniometer attached to the eyepiece tube of the microscope as shown in Figure 10. The Goniometer is a mechanical arrangement that provide a Vernier scale along with circular one that can yield angles with an accuracy of better than 0.25^o. A schematic presentation of all above mentioned angles are shown in Figure 9.

Acknowledgments

Authors are thankful to the technical staffs of the GSI, Darmstadt, Germany for their technical support and information. M. K. Singh is thankful to the University Grants Commission (UGC), Govt. of India, for the funding through UGC D. S. Kothari Post-Doctoral Fellowship (DSKPDF) scheme. V. Singh is thankful to the Department of Science and Technology (DST), New Delhi for constant financial support.

References

[1] P L Jain et al., Phys. Rev. Lett. **48**, 305 (1982).

[2] T Kobayashi et al., Phys. Rev. Lett. **60**, 2599 (1988).

[3] H Geissel et al., Nucl. Instrum. Methods Phys. Res. **B70**, 286 (1992).

[4] T Kubo et al., Nucl. Instrum. Methods Phys. Rev. **B70**, 309 (1992).

[5] B M Sherrill, Prog. Theor. Phys. Suppl. **146**, 60 (2002).

[6] G Rudstam et al., Nucl. Phys. **A21,** 1027 (1966).

[7] K Summerer et al., Phys. Rev. **C42**, 2546 (1990).

[8] K Summerer et al., Phys. Rev. **C61**, 0346071 (2000).

[9] M Mocko et al., Phys. Rev. **C74**, 0546121 (2006).

[10] D K Scott, NATO Advanced Studies Institute on Theoretical Methods in Medium-Energy and Heavy-Ion Physics Proceeding (1978).

[11] F Desk et al., Phys. Rev. **C42**, 1029 (1990).

[12] K Aleklett et al., Heavy Residue Properties in Intermediate Energy Nuclear Collisions with Gold. LBL Report 1990; LBL—29793 DE91 009072 LBL-29793.

[13] U Milkau et al., Phys. Rev. **C44**, 1242 (1991).

[14] M K Singh, Ph. D. Thesis, V. B. S. Purvanchal University, India (2014).

[15] M K Singh et al., Indian J. Phys. **88**, 323 (2014).

[16] M K Singh et al., Pramana J. Phys. **83**, 377 (2014).

[17] N S Chauhan et al., Indian J. Phys. **87**, 1263 (2013).

[18] M K Singh et al., Indian J. Phys. **84**, 1257 (2010); M K Singh et al., Physics International, **1**, 109 (2010).

[19] V Singh, Ph. D. Thesis, Banaras Hindu University, Varanasi, (1998).

[20] H A Bethe et al., Experimental Nuclear Physics (ed. E. Segre) J. Wiley, New York, 253 (1953).

[21] H A Bethe et al., Experimental Nuclear Physics (ed. E. Segre) Wiley, New York 166 (1953).

[22] J H Webb, Phys. Today **3**, 8 (1950).

[23] W Mitchell, Rep. Prog. Phys. **20**, 433 (1957).

[24] M K Singh et al., Indian J. Phys. **87**, 59 (2013).

[25] J Hufner et al., Nucl. Phys. **A290**, 460 (1977).

Table 1: Mean multiplicity values of different projectile fragments [20].

Interaction	**Energy (A GeV)**	$\langle N_{Z\geq 3} \rangle$	$\langle N_{Z=2} \rangle$	$\langle N_{Z=1} \rangle$
^{40}**Ar + Em**	1.1	0.83 ± 0.03	*1.37 ± 0.22*	*1.96 ± 0.08*
^{56}***Fe*** **+ Em**	1.7	3.03 ± 0.06	*1.62 ± 0.05*	*0.85 ± 0.02*
^{84}***Kr*** **+ Em**	0.95	*1.1 ± 0.04*	*1.86 ± 0.06*	*3.00 ± 0.27*
^{139}***La*** **+ Em**	1.2	*1.79 ± 0.09*	*2.39 ± 0.12*	……
^{197}***Au*** **+ Em**	1.0	*2.30 ± 0.08*	*5.22 ± 0.20*	……

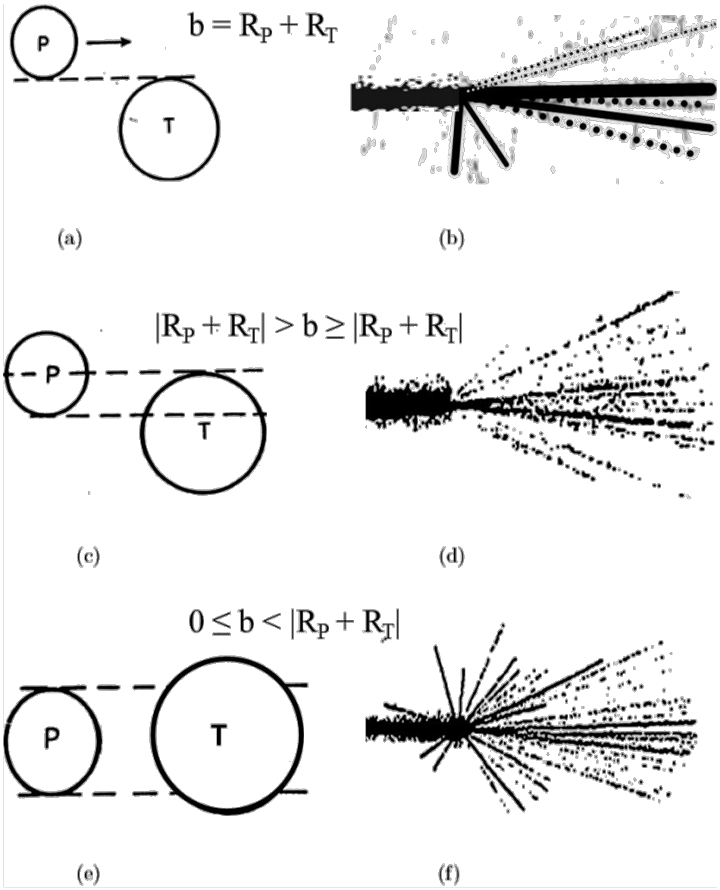

Figure 1: Schematic diagram of (a) peripheral, (c) quasi-central and (e) central collisions and their respectively microphotographs is shown on the right hand side [20].

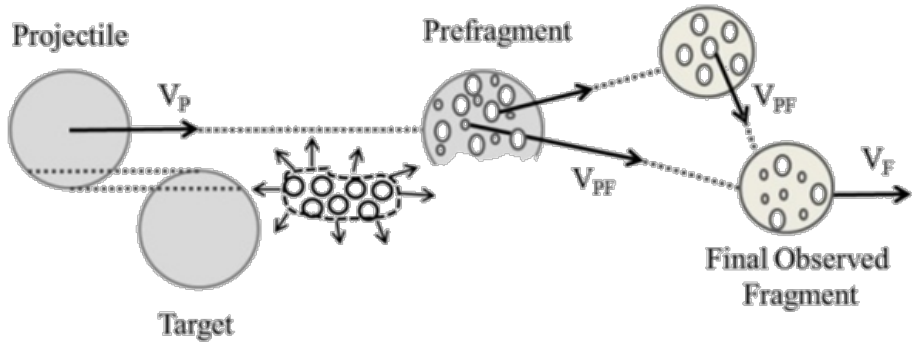

Figure 2: A simplistic picture of the projectile pre-fragmentation and fragmentation processes [20].

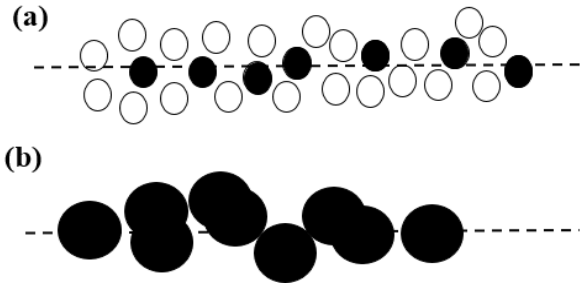

Figure 3: (a) A schematic picture of the latent image formation of charged particle passed through the NED and solid circles represent the path of the charged particle, and (b) shows that the image of the same track after latent image development [20].

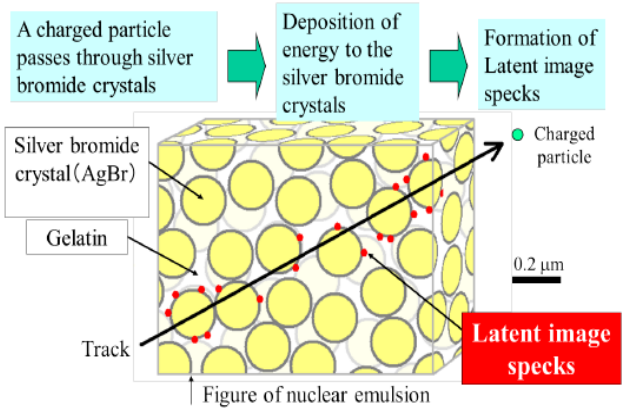

Figure 4: The latent image formation during the exposure to a charged particle [20].

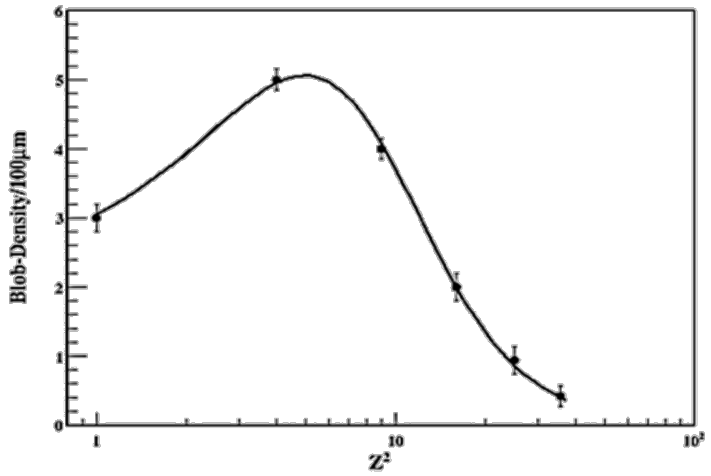

Figure 5: Calibration curve of Blob density as a function of square of the projectile fragments charge (Z^2) [25].

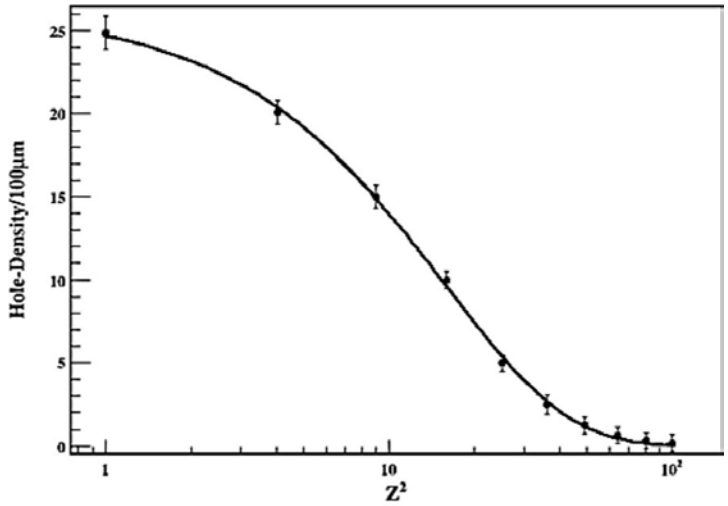

Figure 6: Calibration curve of Hole density as a function of square of the projectile fragments charge (Z^2) [25].

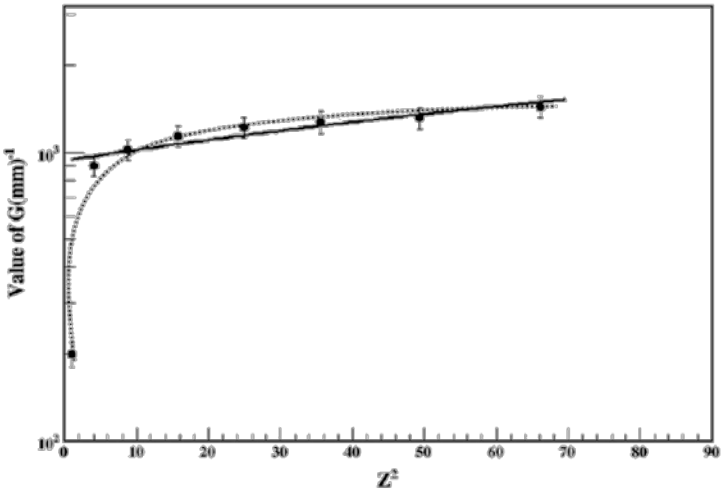

Figure 7: Calibration curve in terms of Gap-length Coefficient as a function of square of the projectile fragments charge (Z^2). Dotted and solid lines, function including and excluding Z=1 data point, respectively, are to just guide the eyes [25].

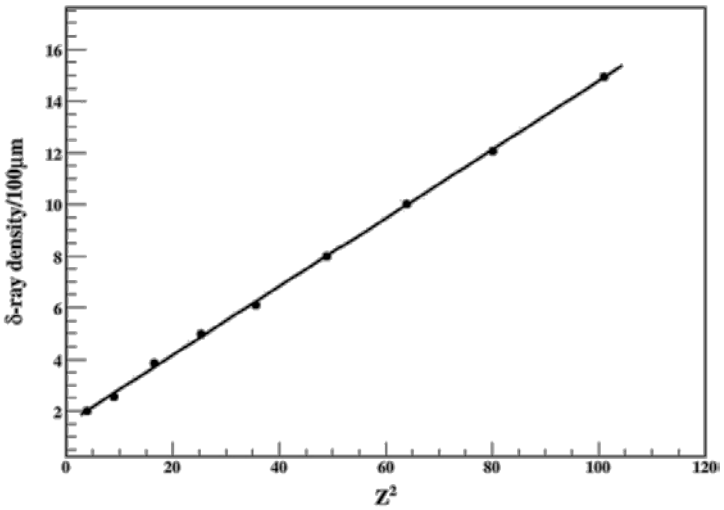

Figure 8: Calibration curve for the medium heavy charge (up to Z = 10) estimation in terms of delta-ray density as a function of (Z^2) [25].

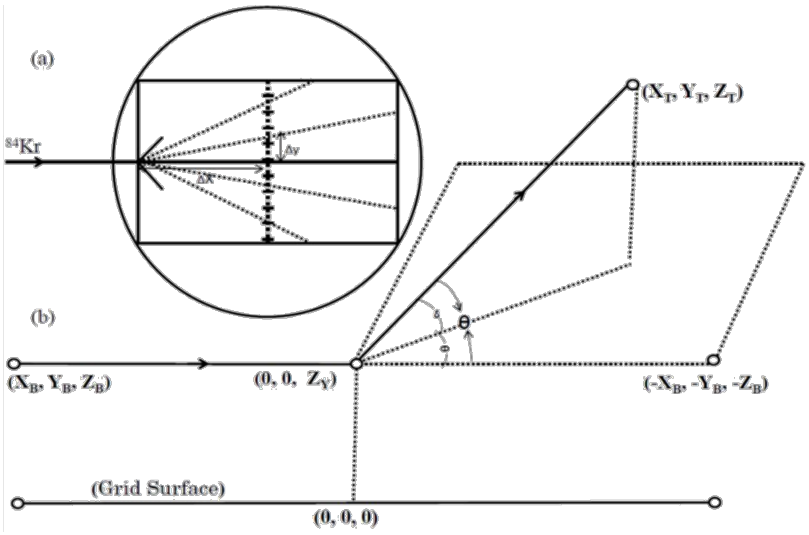

Figure 9: (a) Procedure of the angle measurement and (b) definition of coordinates for angles.

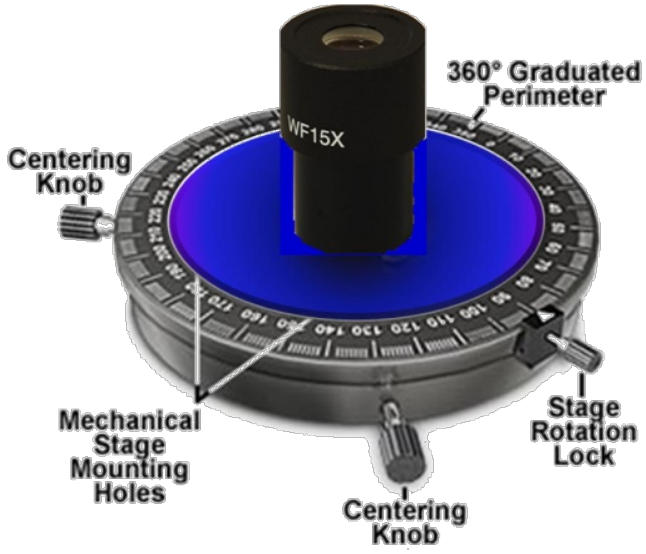

Figure 10: Schematic picture of the Goniometer attached with eyepiece tube.